Cellulose (2024) 31:3589–3606
https://doi.org/10.1007/s10570-024-05847-3

ORIGINAL RESEARCH

Slot-die coating of cellulose nanocrystals and chitosan for improved barrier properties of paper

Ylenia Ruberto · Vera Vivod · Janja Juhant Grkman · Gregor Lavrič · Claudia Graiff · Vanja Kokol

Received: 1 November 2023 / Accepted: 7 March 2024 / Published online: 29 March 2024

Abstract Cellulose nanocrystals (CNCs) and chitosan (Cht) have been studied extensively for oxygen and water vapour barrier coatings in biodegradable, compostable or recyclable paper packaging. However, rare studies have been performed by using scalable, inexpensive, and fast continuous slot-die coating processes, and none yet in combination with fast' and high-throughput near-infrared (NIR) light energy drying. In this frame, we studied the feasibility of a moderately concentrated (11 wt%) anionic CNC and (2 wt%) cationic Cht coating (both containing 20 wt% sorbitol related to the weight of CNC/Cht), by using plain and pigment pre-treated papers. The effect of coating parameters (injection speed, dry thickness settings) were investigated on coating quantity (dry weight, thickness) and homogeneity (coverage), papers' structure (thickness, grammage, density), whiteness, surface wettability, barrier (air, oxygen and water vapour) properties and adhesion (surface strength). The coating homogeneity was dependent primarily on the suspensions' viscosity, and secondarily on the applied coating parameters, whereby CNCs could be applied at 1–2 times higher injection speeds (up to 80 mL/min) and versatile coating weights, but required a relatively longer time to dry. The CNCs thus exhibited outstanding air (4.2–1.5 nm/Pa s) and oxygen (2.7–1.1 cm^3 mm/m^2 d kPa) barrier performance at 50% RH and 22–33 g/m^2 deposition, whereas on top deposited Cht (3–4 g/m^2) reduced its wetting time and improved the water vapour barrier (0.23–0.28 g mm/m^2 d Pa). The balanced barrier properties were achieved due to the polar characteristic of CNCs, the hydrophobic nature of Cht and the quantity of the applied bilayer coating that can provide sustainable paper-based packaging.

Keywords Paper · Nanocellulose · Chitosan · Slot-die coating · Near-infrared (NIR) drying · Barrier properties

Supplementary Information The online version contains supplementary material available at https://doi.org/10.1007/s10570-024-05847-3.

Y. Ruberto · C. Graiff
Department of Life Sciences and Environmental Sustainability, University of Parma, Parma, Italy
e-mail: ylenia.ruberto@unipr.it

C. Graiff
e-mail: claudia.graiff@unipr.it

V. Vivod · V. Kokol (✉)
Faculty of Mechanical Engineering, University of Maribor, Smetanova ulica 17, 2000 Maribor, Slovenia
e-mail: vanja.kokol@um.si

V. Vivod
e-mail: vera.vivod@um.si

J. J. Grkman · G. Lavrič
Pulp and Paper Institute Ljubljana, Ljubljana, Slovenia
e-mail: janja.juhant-grkman@icp-lj.si

G. Lavrič
e-mail: gregor.lavric@icp-lj.si

Introduction

Papers are composed of microfibril cellulose networks, making them inherently porous and highly hydrophilic, which impose challenges in various packaging applications (including pharmaceuticals, food, medical) due to their poor innate barrier performances against gases, water and grease (Adibi et al. 2023; Rastogi & Samyn 2015). Hence, surface coating with bio-based polymers is an emerging and the most common approach to improve these properties (Trinh et al. 2023), also following the circular economy and overall sustainability (Kumar et al. 2021).

The combination of cellulose nanocrystals (CNCs) (Lavoine et al. 2014a, b; Tyagi et al. 2018, 2019) and cellulose nano- and microfibrils (CNFs, CMFs) (native or surface modified; Kumar et al. 2016a, b; Mousavi et al. 2017; Fillat et al. 2023) without, or in combination with polysaccharides, such as chitosan, starch, pectin and alginate, have been studied extensively as candidates for high air and oxygen barrier coatings (Gällstedt et al. 2005; Kopacic et al. 2018; Kansal et al. 2020; Grimaldi et al. 2022) due to their high interaction with oxygen molecules (Saxena et al. 2010), as well as matrices for the integration of other additives (such as antimicrobials, antioxidants, nutrients, etc.) to enhance the papers' functionalities further. The major drawback of polysaccharide based coatings is, however, their low water vapour barrier property, due to their high polarity and intrinsic hydrophilicity. This can be improved slightly by using water insoluble biopolymers, like chitosan (Cht), although the moisture barrier properties of Cht coated paper could be insufficient for, e.g., food packaging applications (Fernandes et al. 2010). Many recent studies have thus been performed by using Cht based emulsions in combination with fatty-acids or waxes, or by the addition of clay to improve hydrophobicity and reduce water vapour transmission rates (WVTR), although often reducing the mechanical properties of the paper (Reis et al. 2011; Trinh et al. 2023). Cht was also applied as a pre-coating on a paper, to provide better bonding and a more uniform surface for other processing steps, such as the subsequent application of a water-insoluble biopolymer by extrusion coating (Koppolu et al. 2019; Kuusipalo et al. 2005). The cationic nature of Cht is, namely, highly favourable for binding strongly with the anionic cellulose fibres, also providing good mechanical and antimicrobial properties to the paper (Bordenave et al. 2010; Song et al. 2018). It has also been shown recently that Cht can indeed lower water absorption, and improve paper smoothness and dry strength (Gatto et al. 2019).

Various coating techniques are employed to apply biopolymers, including nanocellulose, either one or multiple coating layers onto the paper, including extrusion coating, curtain coating, size press coating (Lavoine et al. 2014a, b), rod/blade coating (Lavoine et al. 2014a, b; Afra et al. 2016), and dip coating (Mousavi et al. 2017, 2018). The extrusion coating is still the most conventional process used on the industrial scale for applying thermoplastic polymers, because of the continuous and solvent-free operations that provide a uniform coating without pinholes and cracks, although it suffers from very low coating speed and efficiency (coat weight). On the other hand, the remaining (dispersion and solvent-based) coating techniques have the advantage of requiring low viscous formulations (even in the case of, e.g., size-press coating), but require multiple layers (between 5 and 10) of deposition (dos Santos et al. 2022; Fillat et al. 2023) to cover the base paper's surface fully (generally between 10 and 15 g/m^2), thus to achieve desirable barrier effects (Cranston et al. 2008; Satam et al. 2018). A uniform and relatively-higher coat weight (> 10 g/m^2) at high coating speeds (up to several 10 m/min) can be achieved only in the so-called curtain or slot-die coating process (Rastogi & Samyn 2015; Kumar et al. 2018), as well as blade coating (Mousavi et al. 2018), leading to complete coverage of the paper's surface. The bar/rod coating technique provides better control over the coating thicknesses. However, this method is confined only to the laboratory or pilot scale, and is not considered for scale-up, while, in the case of the dip coating process, it is challenging to control the coating thickness (Rastogi & Samyn 2015).

Both low and high viscosity solutions, including nano- and micro-fibrillated cellulose suspensions (Kumar et al. 2017, 2018), have been tested in a slot-die coating technique. However, very few studies have been performed so far using Cht in such a production process, and, to our knowledge, none in combination with CNCs. Cht-based films' (20–25 µm

thick) production was investigated recently using a simple lab-made slot-die device via a doctor blade (Pemble et al. 2021) fed directly with the 1–2 wt% Cht solution.

Whatever the coating process used, the swelling of base paper fibres is another issue which impacts negatively on the paper's stiffness, due to water penetration into the web structure. This may induce destruction of the fibre-to-fibre bonds, and result in an additional increase of the air permeability (even up to 300%) and thickness (by 6–17 µm) (Lavoine et al. 2014a, b). The drying of the wet deposited layer is, thus, also critical, because dewatering rates affect not only the paper structure (destroy or wrinkle/shrink it), but also the quality (structure) of the final coated layer (Fillat et al. 2023). The results of using conventional drying techniques, including contact drying (Lavoine et al. 2014a, b), hot air (Kumar et al. 2016a, b), infrared Kumar et al. 2016a, b; Mousavi et al. 2018), oven (Mousavi et al. 2017) and room temperature drying (Afra et al. 2016), revealed that a too fast evaporation rate of water from the deposited low-concentrated nanocellulose suspension causes disruption of the coating layer associated to too fast increases in its local viscosity.

In contrast to the conventional drying technologies that have to heat up the substrate surface before the energy also reaches the water molecules in it, the electromagnetic waves of **near-infrared (NIR)** radiation (range from 800 nm up to 1200 nm) can penetrate quickly (in a few sec instead of min by using hot air) and deeply into the coated substrate in the smallest applicable areas. Such an evenly performed heating can activate water molecules directly, and removes them from the entire thickness with extremely short processing times (Griffin et al. 2022). NIR heating has, thus, been introduced as an advanced eco-friendly and high-energy density (>250 kW/m^2) technology to reduce the energy consumption, especially in continuous manufacturing processes like the plastic and paper industries, that require continuous melting or instant drying (Choi et al. 2016). However, no study is yet available on how effective such a highly intensive heating method would be in the drying of biopolymer coated suspensions, nor how it would affect their integrity, uniformity and adhesion to the paper's surface.

In this work, the slot-die deposition technique was thus used to apply a moderately concentrated anionic CNCs' suspension and cationic Cht solution, as well as their mixture, onto the plain and pigment pre-treated papers by a fully automated (computer controlled) laboratory coating device employing high performance NIR energy drying. The effect of the established coating parameters (injection speed and dry thickness settings, at a given slot gap thickness and slot-to-paper distance) in a single (monolayer) and bi-layer deposition, was investigated by the suspension/solution retention properties of the papers, the coating quantity and homogeneity, including the papers' physical (grammage, thickness, density) properties and whiteness. The effect of the papers' structure on the coating adhesion was determined, as well as their barrier properties, focusing on air, oxygen and water vapour permeability, as well as wettability (surface hydrophobicity).

Materials and methods

Materials

Chitosan (MW of 310000–375000 and deacetylation grade of >75%) and acetic acid (HOAc, ACS grade) were purchased from Sigma-Aldrich (St Louis, MO, USA). Cellulose nanocrystals (CNCs) containing 253.5 ± 7.5 mmol/kg of sulphate groups (as evaluated by the National Research Council of Canada) was purchased from CelluForce (Canada, production 2015-011) in the form of a fine powder. The plain (unmodified) paper (44 ± 2 g/m^2, 65 ± 2 µm) and pigment pre-treated (film-pressed formulation containing $CaCO_3$ particles, starch as a binder and carboxymethyl cellulose as a co-binder) paper (51 ± 2 g/m^2, 78 ± 3 µm) of different air permeability were obtained from the industrial production of Papirnica Vevče d.o.o. (Slovenia).

Preparation of the coating suspensions/solution

Three water-based suspensions/solution (Table 1) were prepared by overnight mechanical stirring, to obtain well-suspended CNCs and good solubilised Cht: 11 wt% CNC suspension (pH 6.5), 2 wt% Cht solution prepared with 1% of acetic acid (pH 4.5), and a mixture of 5.5 wt% CNC and 1 wt% Cht (pH 5). To all the suspensions, 20 wt% sorbitol, related to the weight of CNC/Cht, was added as a plasticiser,

Table 1 Characteristics of the cellulose nanocrystals' (CNCs) suspension, chitosan (Cht) solution and their mixture (CNC + Cht) used for coating of both paper substrates

Type and designation	Concentration (wt%)	pH***
CNC	11*	6.5
Cht	2*	5
CNC + Cht	5.5 + 1 = 6.5**	5

*The highest possible concentrations in terms of preparation of well-suspended CNCs and solubilised Cht

**The highest concentration of mixture not to form too large aggregates

***Values after the addition of 20 wt% sorbitol related to the weight of CNC/Cht

to improve their shear thinning and a pressure driven flow through a narrow gap of the slot (Kumar et al. 2016a, b). The pH of the more acidic Cht solution was increased further to a pH of 5 by the addition of NaOH, to prevent possible acid-hydrolysis of the cellulosic fibres and subsequent acid-induced paper ageing. The viscosities of the final suspensions/solution were determined at room temperature using a Haake rotational Viscotester V2 (Thermo Scientific, USA).

Slot-die coating and NIR energy drying

A Challanger 175, semi-pilot & fully automated Sheet-to-Sheet (S2S) coating unit (Norbert Schläfli nsm AG, Switzerland) with an inline integrated 190 mm wide slot-die module (TSE Troller AG, Switzerland) and NIR drying module (drying area of 252 mm and length of 125 mm; NIR252-125 Adphos GmbH, Germany) was used to control the speed of the substrate, the flow rate of the injected suspensions/solutions, and the drying power/time; The equipment used with the setup of the coating experiments is shown in Fig. 1. A slot-die shim of 165 µm thickness was used, while the distance between the substrate and the slot lips was set to 75 µm. The injection/flow speed of the suspension/solution was set in the range between 5 and 80 mL/min (corresponding to a substrate speed between 0.3 and 2.4 m/min), depending on the viscosity of the suspension/solution, while the thickness of the dry deposited layer was in the range between 5 and 12.5 µm. The drying was performed at 5 m/min using an NIR heating module with 7.2 kW of power output within up to 2–6 passes, depending on the amount of applied coating.

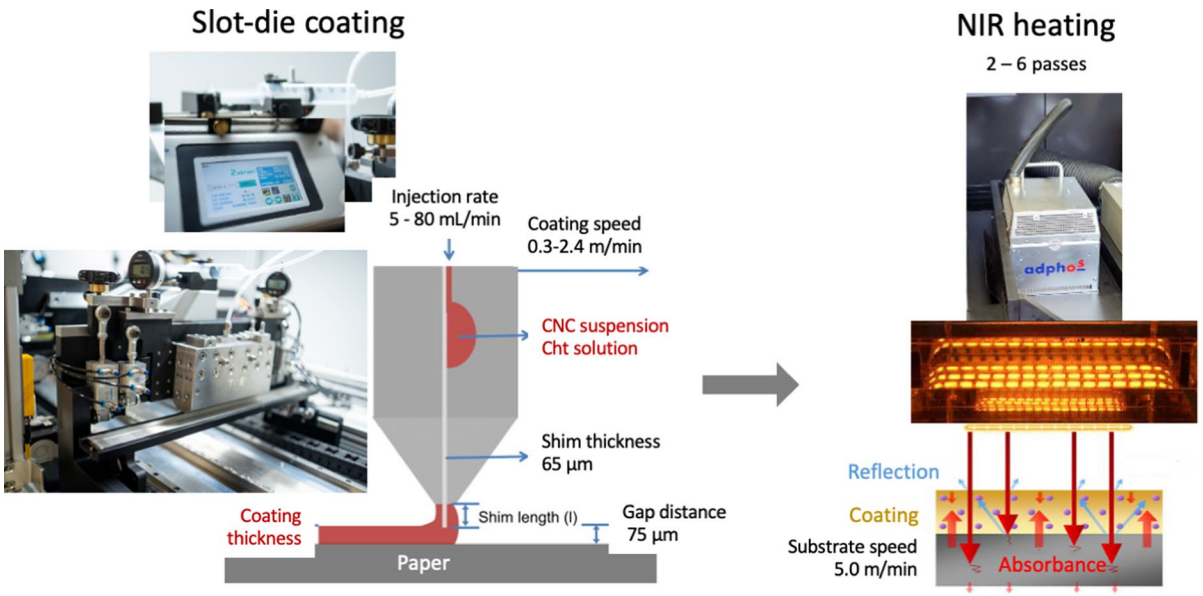

Fig. 1 Schematic presentation of the equipment with the coating experiment's set-up

Fourier Transform InfraRed (FTIR) spectroscopy and microscopy analysis

The FTIR spectra of the uncoated and differently coated papers were performed using a Spectrum one FTIR spectrometer (Perkin-Elmer Inc., USA), with a Golden Gate ATR attachment and a diamond crystal. The spectra were carried out at ambient conditions from accumulating 16 scans at a 4 cm^{-1} resolution over a region of 4000–600 cm^{-1}, and with air spectrum subtraction performed in parallel as a background. The FTIR mapping in the surface area of 2×2 mm with 100 aperture points of 100×100 µm surface areas and a depth of 6.5 µm was performed on selected samples, to evaluate the spatial distribution of the components by using Spotlight 200i Spectrum3 FTIR microscopy (Perkin-Elmer Inc., USA). The Spectrum 5.0.2/10 software program was applied for the data analysis. All the measurements were carried out in duplicate.

Scanning electron microscopy (SEM) imaging

The high-resolution microscope images of uncoated and differently coated papers were performed using an FEG SEM JSM IT800 SHL (JEOL Ltd., USA) microscope.

Water retention properties of papers

The water retention properties of the papers were evaluated with the updated method of (Abo Akademi 1989) using an Abo Akademi Gravimetric Water Retention (AA-GWR) Meter at 23 ± 2 °C and 65 ± 2% RH. The measurement was based on a gravimetric determination of the quantity of the aqueous phase penetrating through the tested paper that was laid onto a filter paper (a standard) with grammage of 413 g/m^2 (Test Blotter Paper, 17 Chr, Noviprofibre, France), and both placed on a hydrophilic Millipore® polycarbonate filter (pore size of 5 µm, Noviprofibre, France). The testing was performed at 90 s of contact time and under an external pressure of 0.5 bar. The presented results are the arithmetic mean values and the Standard Deviations of three independent measurements.

Air flow rate and permeability

The air flow rate (q, mL/min) was measured at 23 ± 2 °C and 65 ± 2% RH by a Bendtsen air permeability tester (Rycobel, Belgium) according to ISO 5636-3:2014, using a pressure of 1.47 kPa at the measuring head. The presented results are the arithmetic mean values and the Standard Deviations of at least ten independent measurements. The air permeability (AP, nm/Pa s) was then calculated by utilising the following equation: $P = 0.0113 \times q$, where q is the mean air flow rate passing through the test area of 1000 mm^2 at a given pressure.

Grammage, thickness, density and coating weight

Following the ASTM D646-96 Standard, 4–6 samples of each uncoated and coated papers were cut into squares of 1 cm^2 (1 cm × 1 cm), conditioned at 23 ± 2 °C and 65 ± 2% RH for at least 24 h, weighed on an analytical scale (AE 240 Analytical Balance, Mettler Toledo). The grammage (G, g/m^2) was calculated from the following Eq.: M/A, where M (g) is the paper's weight, and A (m^2) is the area. The thickness was measured using a Kafer Prec Micrometer 0.001 mm F 1000/30 (Käfer Messuhrenfabrik GmbH & Co. KG, Germany), and expressed as the density (ρ_V, g/cm^3). The presented results are the arithmetic mean values of 4–6 independent measurements with the Standard Deviations. The weight of the coatings (g/m^2) was estimated theoretically, based on the applied total coating mass (CNC vs. Cht including sorbitol) on the application area.

Moisture content

The moisture content evaluation experiment was executed in triplicate. The samples were cut into squares of 1 cm × 1 cm, conditioned at 23 ± 2 °C and $65 \pm$% RH for at least 24 h, and dried in a moisture analyser (DBS 60-3, Kern & Sohn GmbH, Germany; standard drying with automatic switch off) to the absolute dry weight. The moisture content (g H_2O/100 g paper, expressed in %) was calculated ($(M_w - M_d)/M_d \times 100$) from the wet ($M_w$) and absolutely dried ($M_d$) mass, while the time of drying was recorded.

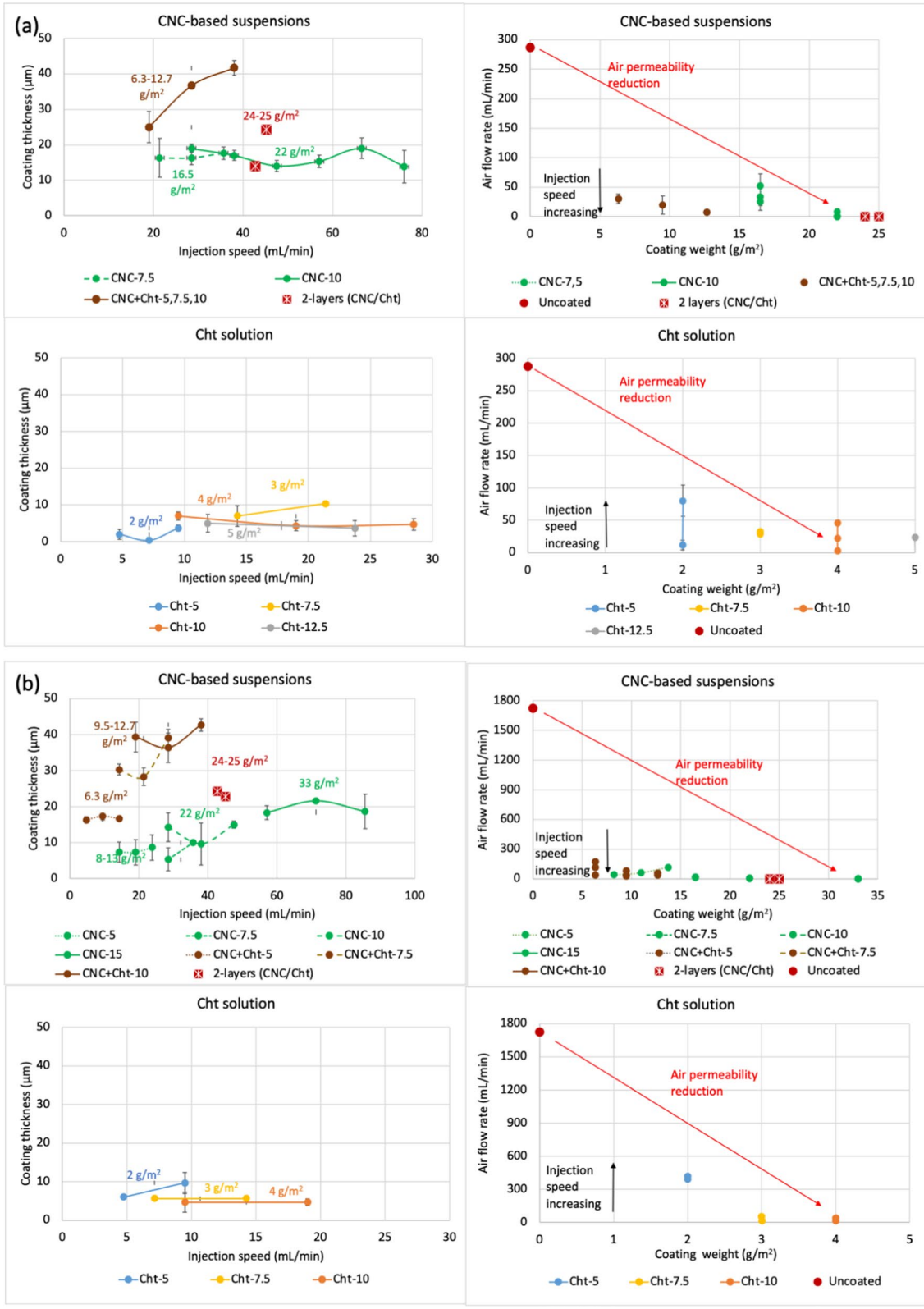
(a)
CNC-based suspensions
Coating thickness (µm)
Injection speed (mL/min)
6.3-12.7 g/m²
24-25 g/m²
22 g/m²
16.5 g/m²
CNC-7.5
CNC-10
CNC+Cht-5,7.5,10
2-layers (CNC/Cht)
CNC-based suspensions
Air flow rate (mL/min)
Coating weight (g/m²)
Air permeability reduction
Injection speed increasing
CNC-7,5
CNC-10
CNC+Cht-5,7.5,10
Uncoated
2 layers (CNC/Cht)
Cht solution
Coating thickness (µm)
Injection speed (mL/min)
2 g/m²
4 g/m²
3 g/m²
5 g/m²
Cht-5
Cht-7.5
Cht-10
Cht-12.5
Cht solution
Air flow rate (mL/min)
Coating weight (g/m²)
Air permeability reduction
Injection speed increasing
Cht-5
Cht-7.5
Cht-10
Cht-12.5
Uncoated
(b)
CNC-based suspensions
Coating thickness (µm)
Injection speed (mL/min)
9.5-12.7 g/m²
24-25 g/m²
33 g/m²
6.3 g/m²
22 g/m²
8-13 g/m²
CNC-5
CNC-7.5
CNC-10
CNC-15
CNC+Cht-5
CNC+Cht-7.5
CNC+Cht-10
2-layers (CNC/Cht)
CNC-based suspensions
Air flow rate (mL/min)
Coating weight (g/m²)
Air permeability reduction
Injection speed increasing
CNC-5
CNC-7.5
CNC-10
CNC-15
CNC+Cht-5
CNC+Cht-7.5
CNC+Cht-10
2-layers (CNC/Cht)
Uncoated
Cht solution
Coating thickness (µm)
Injection speed (mL/min)
2 g/m²
3 g/m²
4 g/m²
Cht-5
Cht-7.5
Cht-10
Cht solution
Air flow rate (mL/min)
Coating weight (g/m²)
Air permeability reduction
Injection speed increasing
Cht-5
Cht-7.5
Cht-10
Uncoated

◂**Fig. 2** Effect of slot-die coating of different CNC-based suspensions and Cht solution on increasing the coating weight (g/m^2) and coating thickness (µm), and reduction of the air flow rate (mL/min) for the **a** plain and **b** pre-treated paper, depending on the coating parameters' settings (i.e. injection speed/5–80 mL/min and dry thickness/5–12.5 µm)

Surface wetting

The water contact angle (CA) was assessed with an OCA25, DataPhysics Instruments (ASTM D5725-99) using a 3 µL drop of milliQ water observed for at least 20 s. The presented results are the arithmetic mean values and the Standard Deviations of at least three independent measurements.

Water vapour transmission rate (WVTR) and permeability (WVP)

The water vapour transmission rate (WVTR, g/m^2·d) was evaluated in duplicate at 23 ± 2 °C and 50 ± 5% RH, according to the ASTM F1249 Standard, using an Extra solution MultiPerm 050 instrument (PermTech srl, Italy). The analysed surface area was 2.01 cm^2. The water vapour permeability (WVP, g mm/m^2 d Pa) was then calculated from the obtained WVTR values by utilising the following equation: WVP = WVTR × l/Δp, where l is the thickness of the coated paper, and Δp is the partial water vapour pressure difference between the two sides of the paper (21.1 mmHg*0.85).

Oxygen transmission rate (OTR) and permeability (OP)

The oxygen transmission rate (OTR, cm^3/m^2 d) was determined on the surface area of 7.069 cm^2 at 23 ± 1 °C and 50 ± 2% RH, using an Oxygen Transmission Rate System PERME® OX2/230 (Labthink Instruments Co., Ltd, China), according to the ASTM D3985 Standard. The values are the average results obtained after 2–3 measurements at an oxygen flux rate of 10 mL/min and pressure of 80 kPa. The upper limit of the oxygen transmission rate tester used is around 65,000 cm^3/m^2 d. The thickness used in the calculation of the oxygen permeability (OP, cm^{3}mm/m^2 d kPa) was the thickness of the coated paper.

CIE whiteness and CIELAB colour measurement

The colours of the paper surfaces, with or without coatings, were measured using a CIE-L*a*b* system with a portable spectro-densitometer, Spectrodens B110040 (Techkon GmbH, Germany). The L* (0/darkness to 100/lightness), a* (− indicates greenness and + indicates redness), and b* values (− indicates blueness and + indicates yellowness) were determined, and the whiteness index was assessed according to UNI-EN 15866:2010 under a D65 illuminant.

Z-directional tensile strength determination

The determination of the z-directional tensile strength was carried out in compliance with the ISO 15754:2009 Standard using the Zwick Roell Z010 tensile testing machine, equipped with a 10 kN measuring cell, and controlled by the testXpert software (Version II V3.2, Zwick GmbH & Co. KG, Ulm, Germany). The testing was conducted on conditioned samples at 23 ± 1 °C and 50 ± 2% RH. The values are the average results obtained after five measurements for each sample.

Results and discussion

The coating efficacy

Slot-die coating is a non-contact coating method, in which the coating fluid is transferred from the slot to the substrate via a fluid bridge (coating meniscus) that crosses the air gap between the slot-die lips and the substrate surface (as shown schematically in Fig. 1). Setting the coating thickness (wet or dry) and injection speed (or substrate speed at a given slot gap/shim thickness and slot-to-substrate distance) are therefore crucial for homogeneous deposition, as these determine the amount of coating applied and its changing with the coating speed (Kumar et al. 2018). The change in paper thickness (%) and air flow rates (mL/min), along with the coating weights (g/m^2), were thus evaluated to assess the coating efficacy.

As seen from Fig. 2a, the (plain) paper thickness increased slightly with the injection speed for all dry coating settings (5, 7.5, 10 and 12.5 µm), and, as expected, given the different dry weights applied (from 6 up to 25 g/m^2). The thickness change was the most significant for CNC + Cht (5.5 + 1 wt%) mixture, resulting in an increase of thickness from 27.6% (at a 19 mL/min injection speed and 5 µm dry thickness setting) to 39.3% (at 38 mL/min and 10 µm dry thickness settings), although the dry weight applied was relatively very low (6.3–12.7 g/m^2); the air flow rate, instead, reduced by around 76.7% (from 30 to 7 mL/min). In the case of the highly concentrated (11 wt%) CNC suspension, the air flow rate was reduced by about 51.1% (from 51.8 to 25.3 mL/min) at 16.5 g/m^2, and further by about 99.8% (from 8.47 to 0.013 mL/min) at 22 g/m^2 weight depositions (achieved at all injections speeds and by setting the dry thickness to 5 and 10 µm, respectively). A similarly low air permeability (3 mL/min) was obtained with a coating of only around 4 g/m^2 (2 wt%) Cht solution (achieved at a much lower injection speed/9.5 mL/min and dry weight setting of 10 µm), confirming the ability of Cht to form a uniform deposition on the paper at appropriate technological parameters.

The coating efficacy on pre-treated paper (Fig. 2b) was similar, although the effect of air permeability reduction was much more significant (due to the fact that this paper exhibits a relatively much higher permeability, probably due to the presence of porous $CaCO_3$ mineral particles) as compared to the plain paper. The air flow rate was, thus, reduced by about 97.8% (from 1724.2 to 37.6 mL/min) already at 6.33 g/m^2 of deposited CNC-Cht mixture (achieved at 14.3 mL/min injection speed and a 5 µm dry thickness setting), while given even a 99% reduction (to 13.3 mL/min) in the case of a 4 g/m^2 deposited Cht solution. The air flow rate was also reduced by 99.6% (to 4.7–6.2 mL/min) at increasing the coating weight of CNCs to 22 g/m^2 (achieved at 47.5 mL/min injection speed and a 10 µm thickness setting), while the paper had very low air permeability (< 1 mL/min) for the applied 33 g/m^2 (obtained at higher injection speeds/57–85 mL/min and 15 µm dry thickness setting).

The results also indicated that a higher viscosity CNC suspension can be applied homogeneously at much higher injection speeds (even up to around 80 mL/min, corresponding to a substrate speed of around 2.4 m/min) as compared to the lower viscosity Cht solution, where it was limited to around 30 mL/min by using such a shim width. This can be explained by the different surface tensions and viscocapillary forces of these liquids, which also limits their operation conditions, and, thus, coating efficacy (Ding et al. 2016). According to the results of the paper thickness difference, the CNCs coating on the plain paper (a 20% increase) was also more superficial than on the pre-treated paper (a 15% increase) at the same (10 µm) dry coating thickness setting and independent of the used injection speed.

For both papers, the 2-layers coating (applying 22 g/m^2 of 11 wt% CNCs, followed by 3 g/m^2 of 2 wt% Cht; giving in total 24–25 g/m^2 of coating weight with a similar increase in thickness) thus made both papers almost air impermeable; the air flow rates reduced to around 0.01 mL/min for the plain and to around 0.5 mL/min for the pre-treated paper.

However, controlling the interactions between the water and the paper structure is crucial for the paper's functional properties, above all, its **damage or shrinkage during the drying process**, which can also contribute to the overall barrier properties. In order to determine the impact of these phenomena, the papers were tested for their structural properties' change after exposure to extreme conditions, i.e. soaking them for 30 min in milliQ water and drying in hot air at 105 °C for 30 min (which was longer than needed to get them dried absolutely). The results, presented in Fig. S1, showed that both papers shrank below 1.1% in both directions, while the thickness increased by about 2.5% (1.7 µm) resulting in about a 2 wt% (1 g/m^2) of increase in their grammage, which means that the effect of shrinkage can be excluded from the evaluation of their functional properties (above all, barrier efficiency).

The NIR heated drying efficacy

As already described in the Introduction, the dewatering of the coated layer is an important aspect of a coating process, which influences both the runnability/coatability of the coating suspension/solution and its drying, originating from the interaction between the paper, the water phase of both the coating suspension/solution and that penetrated into the paper, as well as their **water retention abilities** (Kumar et al. 2016a, b, 2018). That is why

the water retention ability of all the used suspensions/solutions was evaluated on the filter paper (taken as a control), as well as on the tested papers placed onto it.

As seen from the results collected in Table 2, the water retention of the Cht solution by the filter paper was much higher (749 g/m^2) compared to the CNCs suspension (152 g/m^2) of the same viscosity, or their mixture (213 g/m^2). On the contrary, all the suspensions/solution were retained almost completely by both tested papers (739–689, 19–118 and 194–95 g/m^2, respectively) when applied on it. The retention was similar (CNC, Cht), or slightly higher (CNC + Cht) for the plain paper, while it increased significantly (Cht, CNC + Cht) for the pigment pre-treated paper. The latter may be a consequence of the more open structure of this paper (mainly surface and bulk porosity) due to the minerals it contains, which increases the penetrations of the Cht solution and CNC + Cht mixture. Such behaviour can be also supported by an increase of paper thickness (Fig. 1), which was generally higher for the plain paper (between 17–25% for CNC and 2–14% for Cht) as compared to the pre-treated one (7–20% for CNC and 5–10% for Cht). This means that the Cht solution penetrated better into the bulk structure of the papers, while the CNCs remained mainly on their surfaces. This effect was more pronounced on the plain paper's substrate, as is clearly evident from the images obtained by optical microscopy presented in Fig. S2.

Therefore, the retention of the half-less concentrated mixture of CNC + Cht was also lower (19 vs. 118 g/m^2) by the plain paper, although a highly roughened structure, generating a uniform coating, was observed on both papers' surfaces (Fig. S2) due to the formation of aggregates. The formation of aggregated crystalline structures of CNC-Cht dispersed in the Cht solution were formed, due to both poor/part miscibility of those components, and the formation of strong intermolecular hydrogen bonds and electrostatic interactions between the negatively charged/sulphonated CNCs and positive/aminated Cht, deposited mainly on the outer surface of the papers. The thickness of the pre-treated paper thus increased between 27–34%, and even up to 27–40% for the plain paper at similar coating conditions (Fig. 1), although it contributed to the overall decrease in paper densities (Fig. S3).

The water-richer and less concentrated Cht (4 g/m^2) coated papers thus required similarly longer times to dry (up to 3 few seconds long passes were required at 7.2 kW radiation power and 5 m/min substrate speed) by using NIR radiation heating, as compared to the coated CNC-Cht mixture applied with higher coating weights (9.5 g/m^2). The drying time was increased further, even up to 6 passes of NIR heating, when the coating weight of the CNCs suspension was increased to 33 g/m^2 (which corresponded to an increase in paper thickness of about 20 µm). The longer drying times of these samples (pre-conditioned/moisturised at 23 ± 2 °C and 65 ± % RH for 24 h) to an absolute dry weight (from 60/167 s for the uncoated to 180/205 s for differently coated) also support the analyses of moisture content and the time needed for its removal by using a 400 W halogen-quartz glass heater (Fig. S3). In addition to the heating temperature, the distribution of the heating throughout the sample also has an important effect on the drying kinetics and quality. The in-plane temperature distribution under NIR radiation of the sample may be more important for the quality of heating than the through-plane heat conduction, although the latter was more dominant due to the difference in dimensions of the coated/heated paper (i.e. 100–50 µm thick vs. 7 X 20 cm surface area). Accordingly, thicker CNCs coatings with distributed randomly and highly hydroscopic CNCs could affect the poor adhesion of

Table 2 Viscosity and water retention properties of the filter and tested papers related to the differently prepared suspensions/solutions used for the coatings

Suspension/solution	Viscosity (dPa s)	Water retention of the papers		
		Filter	Plain	Pre-treated
CNC (11 wt%)	50 ± 2	152 g/m^2	13 g/m^2	7 g/m^2
			Δ = 139 g/m^2	Δ = 145 g/m^2
Cht (2 wt%)	52 ± 1	749 g/m^2	10 g/m^2	60 g/m^2
			Δ = 739 g/m^2	Δ = 689 g/m^2
CNC (5.5 wt%) + Cht (1 wt%)	25 ± 1	213 g/m2	19 g/m^2	118 g/m^2
			Δ = 194 g/m^2	Δ = 95 g/m^2

the coating to the paper, due to uneven in-plane distribution of the heat and, thus, the retaining of moisture.

The surface chemistry, colouration, whiteness and morphology

Surface chemistry, roughness and surface porosity are other important parameters for the substrate to be coated, as they play a critical role in the final coating uniformity, coverage and anchoring achieved. Since there was a large amount of water in the suspensions/solution, the final coat weights obtained were not high, and, therefore, uniform surface coverage was expected. FTIR (imaging) spectroscopy, SEM imaging, whiteness and CIELAB colour values were used to identify these interdependencies.

Figure 3a shows the **FTIR spectra** for the uncoated papers, CNC, Cht and 2-layers (CNC/Cht) coated papers on both the coated (upper) and uncoated (bottom) sides. The spectra showed the differences between the uncoated and coated papers clearly, as well as the unaltered underside of the papers (indicating that no coating had penetrated through them). The spectra between the uncoated papers and papers coated with CNCs did not show significant differences; the smaller peaks between 1311 and 1376 cm^{-1} for the CNCs coated papers could be attributed to the S=O band from the stretching vibrations of the sulphate groups present on the CNCs, which was reduced for the 2-layers coated papers. The band at around 1644 cm^{-1} was observed in each spectrum, which was due to the vibration of

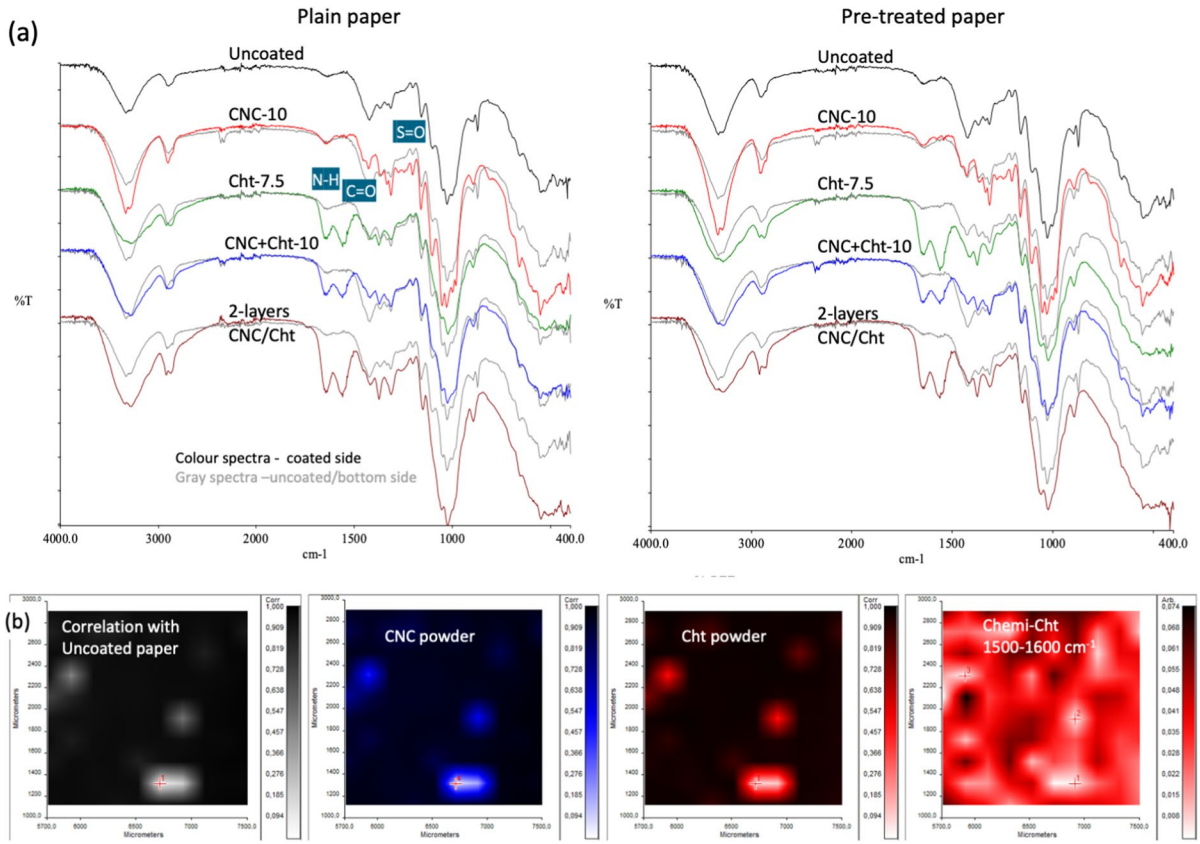

Fig. 3 **a** FTIR spectra of uncoated papers and representative papers coated with (11 wt%) CNC (22 g/m2), 2 wt% Cht (7.5 um), mixture of CNC + Cht (10 um) and 2-layers (11 wt% CNC-10 um and 2 wt% Cht-7.5 um). The colourised spectra represent the upper/coated side, and the grey the opposite/uncoated side of the paper. **b** Micro-FTIR mapping images for 2-layers (CNC and Cht) coated plain paper in correlation with the uncoated paper, CNC and Cht powders, respectively, and chemi-maping for Cht in the amide region (between 1500 and 1600 cm^{-1}), all obtained from 100 positions of 200 × 200 µm in depths of 6.7 µm for a 2 × 2 mm surface area of the papers

C=O in the glucose ring of the cellulose, and which overlapped with the carbonyl stretch in the amides and getting intensified for the Cht coated papers. In addition, the band at around 1561 cm^{-1} was observed only for papers coated with Cht, which was due to the bending vibrating of the N–H in amino groups (Zakaria et al. 2015). The lowering of the intensities of these two bands (related to the uncoated papers' sides), and proportional changing of the intensity of the O–H vibrational band centred at around 3330 cm^{-1}, suggesting a different (still rather smaller) penetration of Cht into the papers, as well as the involving of these groups in the hydrogen bonding. Although the highly soluble and flowable Cht solution might penetrate into the paper via capillary action, an increase in the number of less-concentrated Cht coating layers would be required to fill the pores and cover the paper's surface by the film-forming capacity, as already established by previous studies (Tanpichai et al. 2022; Fernandes et al. 2010; Kansal et al. 2020; Bordenave et al. 2007, 2010). On the other hand, a change in the intensities of the amide peaks for Cht in the 2-layers coated papers over the surface can be also observed from the FTIR chemi-mapping microscopy analysis (Fig. 3b), indicating its coating inhomogeneity being more prominent for the plain paper; the spatial distribution of CNC, on the contrary, was more homogeneous for the analysed sample. A strong intermolecular hydrogen bonding and electrostatic interactions between the amino groups of the glucosamine monomers of Cht and hydroxyl/sulphur groups of the glucoside units in the cellulose fibres and CNCs can be also confirmed from the FTIR spectra (Fig. 3a) for both the mixture (5.5CNC + 1Cht) and 2-layers coated papers. Anyway, there were no differences observed in the spectra between the uncoated (plain vs. pre-treated) papers (Fig. S4) to examine the influence of the presence of pigments on the coating efficacy.

SEM imaging was performed to observe the morphological surface and cross-section structure of the papers before and after the selected coatings. As shown in Fig. 4a, comparing the uncoated papers, the fibres in the pigment pre-treated paper had a rougher surface than the plain, and resulted in an even more compact and full coverage of the 22 g/m^2 CNCs deposition. Both papers showed an even smoother surface after applying the Cht. The cross-section images (Fig. 4b) examined the adhesion of the CNC/Cht coated layer and its evenness over the papers' surfaces, confirming the uniform drying of the samples.

The whiteness (Fig. 5) and **CIELAB colour measurements** (Fig. S5) with a low variation of Standard Deviation for the 6 measurements performed additionally confirmed the uniformity and homogeneity of the coatings. A small reduction in lightness (L*), redness (a^*) and yellowness (b^*) for differently CNC-coated papers as compared to the uncoated ones can be observed, while no changes for the papers coated with Cht; the average colour values between the coated and uncoated papers for all samples were less than 3, which is not perceptible to the human eye. The whiteness, on the other hand, increased significantly for the CNC-coated papers (even up to 23% for a 20 µm thick coating of 22–33 g/m^2; from 78 to 94 for the plain, and from 80 to 99 for the pre-treated paper) and given a shining effect.

The surface wettability and water vapour permeability

The coating efficacy was expected to correlate with the changes in surface wetting and water permeability values. Figure 5 shows the surface wetting (evaluated by contact angle/CA measurement) and WVTR values of differently coated papers, which correlated well with their moisture retention properties presented in S3. Both the plain and pre-treated papers were found to be highly permeable for water vapour, so the WVTR tests failed. Instead, the CA of the pre-treated paper was relatively higher (118°) than that of the plain paper (85°), indicating its different hydrophilic nature on the surface, which may affect the spreading, absorption and adhesion of the coated CNC and Cht suspensions/solution. Slightly higher suspensions/solution retention properties for the plain paper (Table 2) were thus expected, to ensure quicker absorption of the water-rich suspensions/solution and influence the higher adhesion, also having an effect on the WVTRs.

Indeed, for both CNC coated papers, the CA was reduced to around 40° by increasing their coating weight (from 6 to 33 g/m^2), while the WVTR was decreased from the unmeasured (for untreated papers) up to 136–128 g/m^2d. This confirmed again the retention of highly hydrophilic CNC, mainly on the paper surface, as already confirmed by FTIR analysis (Fig. 3) and SEM imaging (Fig. 4).

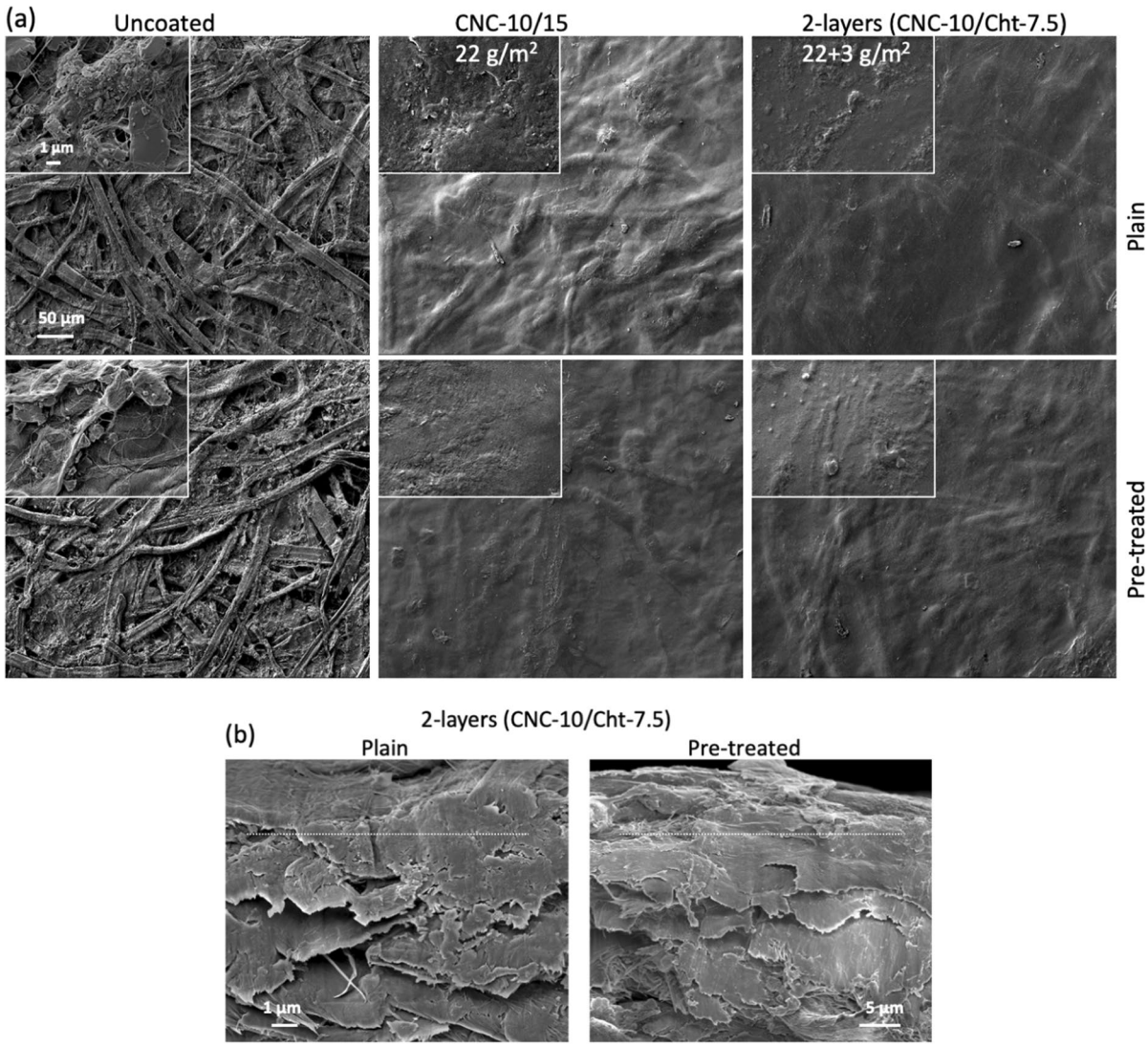

Fig. 4 SEM imaging of the uncoated and differently coated papers **a** surface and **b** cross-sections

The Cht solution (2–5 g/m^2) penetrated more deeply into the papers, that reduced the WVTR values slightly (48–67 g/m^{2}d), while exhibiting moderate hydrophobicity (an increase up to 102° for plain paper at the highest 5 g/m^2 deposition, and reduced it up to 88° for the pre-treated paper). The deposition of (9.5 g/m^2) CNC-Cht mixture did not have a significant effect on any of the properties, due to the formation of aggregates and their uneven distribution over the paper's surface. According to previous studies, up to 3 Cht layers (of 13.7–20 g/m^2 coated weight) were required to fill the paperboard surface pores, making the paper matrix fully saturated, thus reducing the WVTR to 49 g/m^{2}d (dos Santos et al. 2022) by controlling the interactions with the water molecules (Bordenave et al. 2007). On the contrary, the 2-layer coated samples thus resulted to a CA of 84–93° (which could be associated with the hydrophobic nature of chitosan), and WVTR of 68–70 g/m^{2}d, due to controlled interactions with the water molecules.

It can be concluded that both CNCs and Cht contributed to the air permeability reduction, where the CNCs generated a highly hydrogen-bonded

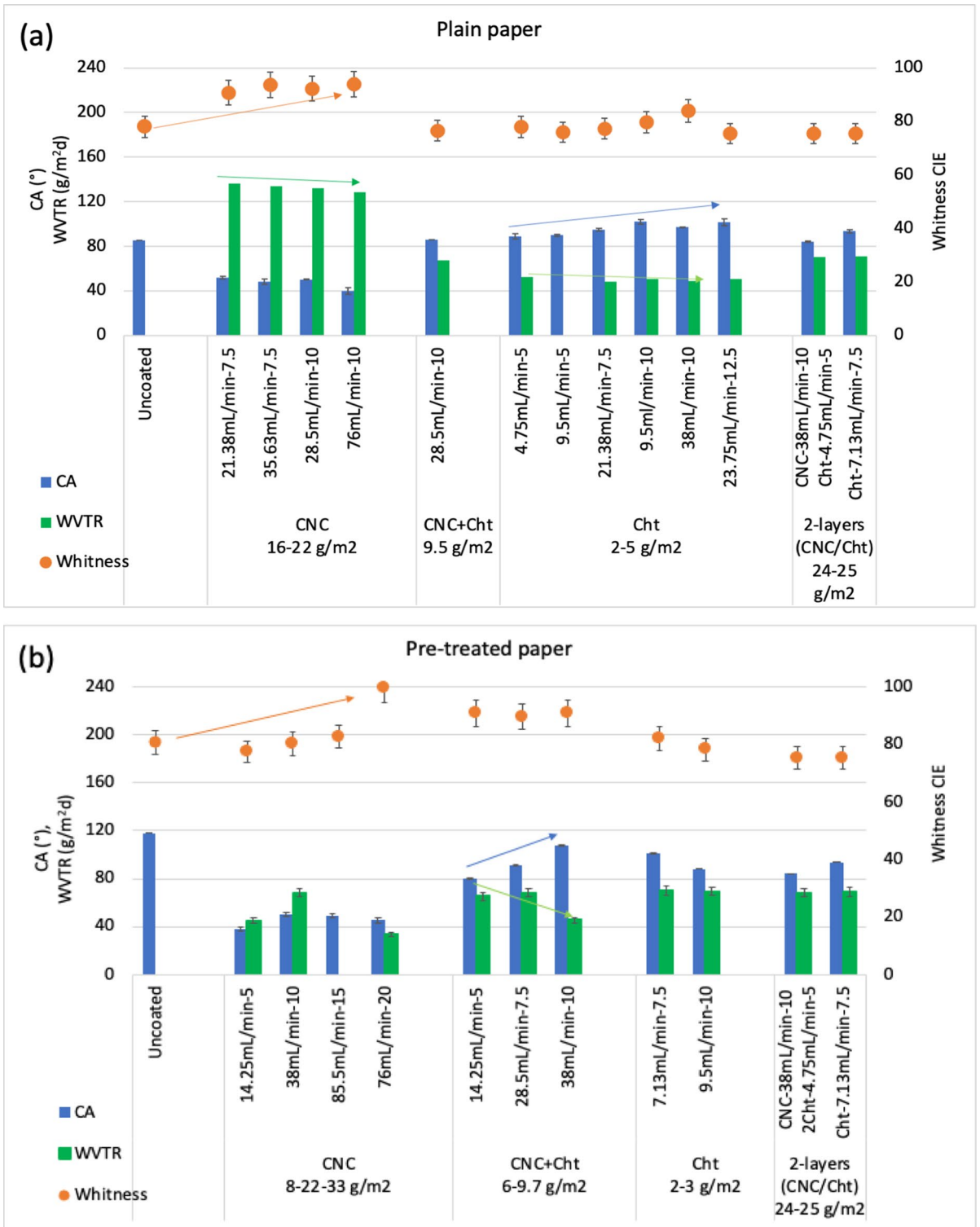

Fig. 5 Whiteness, contact angle (CA), and water vapour transmission rate (WVTR) values for (a) plain and (b) pre-treated paper, depending on the coating parameters and the applied coating weights

network with the paper, while eletrostatic interaction with the Cht applied on top, reduced the paper surface wettability and WVTR. The random orientations of the polymer chains of Cht, their free volume and swelling by water, thus reduced the moisture permeation by sorption of the vapour molecules (Trinh et al. 2023).

Air and oxygen permeability

The oxygen barrier is another essential property of coated materials, as it prevents detrimental contact between the product and the environment, thereby decreasing the rate of oxidation of food or pharmaceutical products, and ultimately protecting them from spoilage. The oxygen barrier properties are typically evaluated by permeation testing under static state flux; the partial pressure gradient drives the oxygen molecules to diffuse through materials, similar to the diffusion of water vapour molecules. In order to obtain an oxygen barrier it is necessary to obtain an air permeance of < 1 nm/Pa s, as stated by (Kjellgren et al. 2006; Hult et al. 2010), so only the selected papers were studied for oxygen permeability. On the other hand, material is defined as "high oxygen barrier" if its OTR value is less than 3 cm^3/m^2d (at 25 °C, 50% RH) for a 25 µm thick film (Hult et al. 2010), meaning its OP is close to zero.

As can be observed from the data collected in Table 3, the Cht coating of 3–4 g/m^2 already improved the air and oxygen barrier capabilities of the papers significantly by values of 33.9–37.6 nm/Pa s and 21.8–22.8 cm^3 mm/m^2 d kPa, respectively, given the fact that the uncoated papers were too permeable to be measured. The air and oxygen permeability values obtained are comparable to those reported previously by (Kjellgren et al. 2006), who reported air permeability values between 30 and 0.001 nm/Pa s and oxygen permeability between 160 and 0.0006 cm^3 mm/m^2 d kPa, respectively, for the same unbleached and greaseproof papers coated with 1.2–5.2 g/m^2 of Cht; both values thus decreased significantly as the coat weight of the Cht increased. In the pilot-scale coating trials performed, the Cht coat weights obtained were too low (0.2 g/m^2) to seal the pores in the base papers and give an oxygen barrier.

The CNCs provided an even higher oxygen barrier, with up to 2.7–1.0 cm^3 mm/m^2 d kPa of oxygen permeability, accrued from intra- and intermolecular hydrogen bonding and the formation of a more tightly packed crystallinity network within the paper fibres, which coincided well with the previous studies. For example, a significant reduction of oxygen permeability was reported, to 0.003 cm^3 µm/m^2 d kPa for CNCs coated papers, which was lower than the

Table 3 Water vapour (WVP), air (AP) and oxygen (OP) permeabilities of differently coated papers

Paper	Coated suspension/solution	Coat weight (g/m^2)	WVTR* (g/m^2 d)	WVP* (g mm/m^2 d Pa)	AP (nm/Pa s)	OTR** (cm^3/m^2 d)	OP** (cm^3 mm/m^2 d kPa)
Plain of 44 g/m^2	CNC (11 wt%)	22	131.96	0.421	4.18 ± 0.2	2702 ± 45	2.70 ± 0.05
	Cht (2 wt%)	4	50.67	0.141	33.9 ± 1.3	21,792 ± 54	21.79 ± 0.4
	2-layers CNC (11 wt%)						
	Cht (2 wt%)	24	71.16	0.256	0.11 ± 0.1	478 ± 12	0.48 ± 0.01
	Cht (2 wt%)	25	70.26	0.237	0.11 ± 0.1	257 ± 8	0.257 ± 0
Pigment pre-treated of 51 g/m^2	CNC (11 wt%)	22	68.17	0.249	531.1 ± 10	Over range	Over range
		33	n.d	n.d	1.50 ± 0.3	1006 ± 29	1.07 ± 0.03
	Cht (2 wt%)	3	69.89	0.228	37.63 ± 1.2	21,464 ± 784	22.81 ± 0.78
	2-layers CNC (11 wt%)						
	Cht (2 wt%)	24	68.82	0.288	6.65 ± 0.5	16,713 ± 282	16.71 ± 0.15
	Cht (2 wt%)	25	68.21	0.278	5.78 ± 0.4	8220 ± 97	8.73 ± 0.10

*Testing performed at 23 °C and 50% RH; one sample was tested

**Testing performed at 23 °C and 50% RH

commercialised oxygen barrier ethylene vinyl alcohol (EVOH) under dry conditions (Li et al. 2013). Both CNCs, as well as microcrystalline glucan (MCG), were also very effective at relatively high humidity (Adibi et al. 2022a, b; Herrera et al. 2017). The high polarity of CNC associated with the hydroxyl functional groups thus prevent an easy diffusion and passage of oxygen through the coating,as opposed to the Cht only based coating. However, the type of paper (above all its porosity and pre-treatment) also play a role, as, for the pigment pre-coated paper, the air permeability increased highly, and the oxygen permeability could not be measured for a 22 g/m^2 coat weight of CNCs on such a paper, while resulting in an obvious decrease of both values (1.5 nm/Pa s and 1.07 cm^3 mm/m^2 d kPa) when 33 g/m^2 of solids were applied.

The oxygen permeability was additionally reduced (0.48–0.26 and 16.7–8.73 cm^3 mm/m^2 d kPa) for the 2-layers coated papers. The results suggest that there are very few connected pores through the cross-section of such a coated paper, and that highly crystalline CNCs in combination with a Cht layer may form a more compact packing and sealing of the pores of the plain paper, lowering the air and oxygen permeability, as compared to the pre-treated paper. This reduction may also result from the closure of the eventual residual nanopores (by applying Cht) on the papers' surfaces being still present after the CNCs' deposition, both acting as oxygen barrier/blocking materials by creating a more complicated passage for the oxygen molecules. In the case of paper pre-modified with pigments, a slight increase of both air and oxygen permeability values was still observed, which could be due to a too low amount of deposited CNCs (22 g/m^2) for this type of paper (as is evident from the results of the CNCs only coated samples) to fill up the surface structure containing generally more oxygen-permeable $CaCO_3$ particles. An introduction of MCG into a natural rubber (NR) coated paper also resulted in 55% lower oxygen permeability values than pure NR-coated paper, due to a higher hierarchy of the non-permeable crystalline structures of MCG particles, which induced a packed layer through the coating, and thus increased the path length for the oxygen diffusion (Adibi et al. 2022a, b).

Polymers have an excellent oxygen barrier performance when they possess molecular structures that cause polar-polar interactions or hydrogen bonding interaction with oxygen, although, on the other hand, they usually suffer from insufficient WV barrier properties (Lagaron et al. 2013), both being affected greatly by the temperature and RH of the surrounding environment. Generally, as the relative humidity increases, the moisture molecules plasticise the polymer used as the coating, which subsequently enhances the mobility and the extensive mass transfer of oxygen molecules across the film. A high humidity (> 50% RH) thus has a deleterious effect on the oxygen barrier properties (10,000-times higher) of films prepared from MFC (Aulin et al. 2010); the absorption of the water molecules into the cellulose fibrils disrupted the hydrogen bonding networks and weakened the interaction between the fibrils, which fills up the free volumes through the paper base fibres, consequently increasing the permeation paths for the oxygen molecules (Adibi et al. 2022a, b; Herrera et al. 2017). On the other hand, strong hydrogen bonding mediated interlocking between the base paper fibres and polar biobased polymers (as sorbitol was being added; Kumar et al. 2018) could also prevent the coated paper from swelling at high humidity. This can be supported by a study of (Hult et al. 2010), where CMF was applied as a first layer under the hydrophobic shellac, resulting in high OTR (4466–5438 cm^3/m^2 d) and WVTR (6–8 g/m^{2}d) barrier properties.

The improvement of barrier properties to oxygen and WV permeability in comparison to some other studies are collected in Table S1.

Adhesion strength

The performance of the coating is also highly dependent on the adhesive strength and chemical interaction between each level of layers and with the substrate (Trinh et al. 2023). Good adhesion between the coating and base paper is essential, to ensure that the coating remains securely bonded to the paper surface, preventing delamination or flaking. It can also enhance the paper's durability, allowing it to withstand various post-finishing processes, while influencing factors such as glossiness and texture. Finally, the adhesion is also crucial for creating a continuous and uniform barrier layer, required to protect it against moisture, gases, or other external factors.

Coating adhesion to the substrate was quantified with z-directional tensile strength measurement of/

Table 4 Z-directional tensile strength values (N) of the papers before and after selected coatings

Suspension	Coating weight (g/m^2)	Plain paper	Pre-treated paper
Uncoated	–	400 ± 22	435 ± 21
CNC (11 wt%)	22	451 ± 19	456 ± 22
CNC (5.5 wt%) + Cht (1 wt%)	13	414 ± 20	427 ± 20
2-layers CNC (11 wt%)/Cht (2 wt%)	25	464 ± 23	443 ± 22

on selected coated papers. As can be observed from the strength values collected in Table 4, in which the results of the mean values of the measured forces obtained during the determination of the z-directional tensile strength are displayed, a slight increase in forces for the CNCs coated samples and their further increase for 2-layers coated samples were achieved for the same paper by the tested samples. Subsequent visual inspection also revealed the separation of the top Cht layer from the pre-coated CNC for the plain paper (Fig. S6), which was not the case for the pigment pre-treated sample. Separation is visible in the form of white spots (thin pieces of coating) that detached from the surface of the tested sample and adhered to the surface of the adhesive tape. In contrast, if there were no separation, the surface of the adhesive tape would remain uniform and free of particles.

It can be summarised that the applied CNC coatings affect the surface strength of the papers slightly, while the force required for separating the coating from the base paper is, on average, practically the same as for the separation (a kind of delamination) of the uncoated papers. The CNCs proved to be a good adhesive with both the papers.

Conclusions

The slot-die coating was shown to be a suitable technique for the homogeneous deposition of a moderately concentrated CNC suspension on the paper, and in combination with a highly intensive NIR drying method, to allow the formation of a compact film. The coating performance evaluation results indicated that the anionic CNCs adhered strongly with the cellulose fibres of both the plain and pigment pre-treated paper substrates, while the cationic Cht deposited onto it strongly. At sufficiently thick depositions (dry weight applied), such bi-layer coatings can improve the barrier property of papers significantly versus air, oxygen and water vapour. This study indicated that the CNC/Cht coatings can provide sustainable and biodegradable paper-based packaging alternatives, enabling papers' recycling.

Author contributions YR & VV: Investigation, Formal analysis, Data curation. JJG & GL: Methodology, Investigation, Formal analysis, Data curation, Writing – original draft. CG: Investigation, Formal analysis, Funding acquisition. VK: Conceptualisation, Funding acquisition, Methodology, Investigation, Visualisation, Writing – original draft, Writing – review & editing. VV: Investigation, Formal analysis, Data curation.

Funding This research has received funding from the Slovenian Research and Innovation Agency (Research Programme P2-0424). The authors also acknowledge the use of the research equipment Challanger 175 fully automated coating device and the FEG SEM JSM IT800 SHL microscope, procured within the operation "Upgrading national research infrastructures – RIUM", which was co-financed by the Republic of Slovenia and the European Union from the European Regional Development Fund.

Data and materials availability Datasets and materials can be assessed by contacting the Corresponding author.

Declarations

Conflict of interest The authors declared no conflicts of interest.

Ethical approval This declaration is not applicable.

References

Adibi A, Valdesueiro D, Mok J, Behabtu N, Lenges C, Simon L et al (2022a) Sustainable barrier paper coating based on alpha-1,3 glucan and natural rubber latex. Carbohydr Polym 282:119121

Adibi A, Valdesueiro D, Simon L, Lenges CP, Mekonnen TH (2022b) High barrier sustainable paper coating based on engineered polysaccharides and natural rubber. ACS Sustain Chem Eng 10(32):10718–10732

Adibi A, Trinh BM, Mekonnen TH (2023) Recent progress in sustainable barrier paper coating for food packaging applications. Prog Org Coat 181:107566

Afra E, Mohammadnejad S, Saraeyan S (2016) Cellulose nanofibrils as coating material and its effects on paper properties. Prog Org Coat 101:455–460

Akademi A (1989) Tappi J 72(12)

Aulin C, Gällstedt M, Lindström T (2010) Oxygen and oil barrier properties of microfibrillated cellulose films and coatings. Cellulose 17:559–574

Bordenave N, Grelier S, Pichavant F, Coma V (2007) Water and moisture susceptibility of chitosan and paper-based materials: structure–property relationships. J Agric Food Chem 55:9479–9488

Bordenave N, Grelier S, Coma V (2010) Hydrophobization and antimicrobial activity of chitosan and paper-based packaging material. Biomacromol 11:88–96

Choi JW, Chun WP, Oh SH, Lee KSI (2016) Experimental studies on a combined near infrared (NIR) curingsystem with a convective oven. Porgress in Organic Coating 91:39–49

Cranston ED, Gray DG (2008) Birefringence in spin-coated films containing cellulose nanocrystals. Colloids Surf A 325:44–51

Ding X, Liu J, Tal H (2016) A review of the operating limits in slot die coating processes. AIChE J 62(7):2508–2524

dos Santos JWS, Garcia VAdS, Venturini AC, Rad C, da Silva CF, Yoshida CMP (2022) Sustainable coating paperboard packaging material based on chitosan, palmitic acid, and activated carbon: water vapor and fat barrier performance. Foods 11:4037

Fernandes SCM, Freire CSR, Silvestre AJD, Desbrières J, Gandini A, Neto CP (2010) Production of coated papers with improved properties by using a water-soluble chitosan derivative. Ind Eng Chem Res 49:6432–6438

Fillat U, Vergara P, Villar JC, Gomez N (2023) Structural properties of coated papers with cellulosic nanofibres using different metering systems and drying technologies. Prog Org Coat 179:107543

Gällstedt M, Brottmon A, Hedenqvist MS (2005) Packaging-related properties of protein- and chitosan-coated paper. Packag Technol Sci 18:161–170

Gatto M, Ochi D, Yoshida CMP, Ferreira de Silva C (2019) Study of chitosan with different degrees of acetylation as cardboard paper coating. Carbohydr Polym 210:56–63

Griffin R, Hooper K, Cecile C, Jenny B (2022) Comparative study of radiative heating techniques for fast processing of functional coatings for sustainable energy applications. Johnson Matthey Technol Rev 66(1):32–43

Grimaldi M, Pitirollo O, Ornaghi P, Corradini C, Cavazza A (2022) Valorization of agro-industrial byproducts: extraction and analytical characterization of valuable compounds for potential edible active packaging formulation. Food Pack Shelf Life 33:100900

Herrera MA, Mathew AP, Oksman K (2017) Barrier and mechanical properties of plasticized and cross-linked nanocellulose coatings for paper packaging applications. Cellulose 24:3969–3980

Hult EL, Iotti M, Lenes M (2010) Efficient approach to high barrier packaging using microfibrillar cellulose and shellac. Cellulose 17:575–586

Kansal D, Hamdani SS, Ping R, Sirinakbumrung N, Rabnawaz M (2020) Food-safe chitosan-zein dual-layer coating for water- and oil-repellent paper substrates. ACS Sustain Chem Eng 8:6887–6897

Kjellgren H, Gällstedt M, Engström G, Jörnström L (2006) Barrier and surface properties of chitosan-coated grease-proof paper. Carbohydr Polym 65:453–460

Kopacic S, Walzl A, Zankel A, Leitner E, Bauer W (2018) alginate and chitosan as a functional barrier for paper-based packaging materials. Coatings 8(7):235

Koppolu R, Lahti J, Abitbol T, Swerin A, Kuusipalo J, Toivakka M (2019) Continuous processing of nanocellulose and polylactic acid into multilayer barrier coatings. ACS Appl Mater Interfaces 11:11920–11927

Kumar V, Nazari B, Bousfield DW, Toivakka M (2016a) Rheology of microfibrillated cellulose suspensions in pressure-driven flow. Appl Rheol 26:43534

Kumar V, Elfving A, Koivula H, Bousfield D, Toivakka M (2016b) Roll-to-roll processed cellulose nanofiber coatings. Ind Eng Chem Res 55:3603–3613

Kumar V, Koppolu VR, Bousfield D, Toivakka M (2017) Substrate role in coating of microfibrillated cellulose suspensions. Cellulose 24(3):1247–1260

Kumar V, Bousfield D, Toivakka M (2018) Slot die coating of nanocellulose on paperboard. TAPPI J 17(01):11–19

Kumar R, Verma A, Shome A, Sinha R, Sinha S et al (2021) Impacts of plastic pollution on ecosystem services, sustainable development goals, and need to focus on circular economy and policy interventions. Sustainability 13(7):9963

Kuusipalo J, Kaunisto M, Laine A, Kellomäki M (2005) Chitosan as a coating additive in paper and paperboard. Tappi J 4:17–21

Lagaron JM, Catalá R, Gavara R (2013) Structural characteristics defining high barrier properties in polymeric materials. Mat Sci Tech 20(1):1–7

Lavoine N, Desloges I, Khelifi B et al (2014a) Impact of different coating processes of microfibrillated cellulose on the mechanical and barrier properties of paper. J Mater Sci 49(7):2879

Lavoine N, Bras J, Desloges I (2014b) Mechanical and barrier properties of cardboard and 3d packaging coated with microfibrillated cellulose. J Appl Polym Sci 13:40106

Li F, Biagioni P, Bollani M, Maccagnan A, Piergiovanni L (2013) Multi-functional coating of cellulose

nanocrystals for flexible packaging applications. Cellulose 20(5):2491–2504
Mousavi SMM, Afra E, Tajvidi M, Bousfield DW, Dehghani-Firouzabadi M (2017) Cellulose nanofiber/carboxymethyl cellulose blends as an efficient coating to improve the structure and barrier properties of paperboard. Cellulose 24:3001–3014
Mousavi SMM, Afra E, Tajvidi M et al (2018) Application of cellulose nanofibril (CNF) as coating on paperboard at moderate solids content and high coating speed using blade coater. Prog Org Coat 122:207
Pemble OJ, Bardosova M, Povey IM, Pemble ME (2021) A slot-die technique for the preparation of continuous, high-area, chitosan-based thin films. Polymers 13:1566
Rastogi VK, Samyn P (2015) Bio-based coatings for paper applications. Coatings 5(4):887–930
Reis AB, Yoshida CMP, Reis APC, Franco TT (2011) Application of chitosan emulsion as a coating on Kraft paper. Polym Int 60:963–969
Satam CC, Irvin CW, Lang AW, Jallorina JCR et al (2018) Spray-coated multilayer cellulose nanocrystal-chitin nanofiber films for barrier applications. ACS Sustain Chem Eng 6:10637–10644
Saxena A, Elder TJ, Kenvin J, Ragauskas AJ (2010) Highly oxygen nanocomposite barrier films based on xylan and nanocrystaline cellulose. Nano-Micro Lett 2:235–241
Song Z, Li G, Guan F, Liu W (2018) Application of chitin/chitosan and their derivatives in the papermaking industry. Polymers 10(4):389
Tanpichai S, Srimarut Y, Woraprayote E, Malila Y (2022) Chitosan coating for the preparation of multilayer coated paper for food-contact packaging: wettability, mechanical properties, and overall migration. Int J Bio Macrom 213:534–545
Trinh BM, Chang BP, Mekonnen TH (2023) The barrier properties of sustainable multiphase and multicomponent packaging materials: a review. Prog Mater Sci 133:101071
Tyagi P, Hubbe MA, Lucia L, Pal L (2018) High performance nanocellulose-based composite coatings for oil and grease resistance. Cellulose 25:3377–3391
Tyagi P, Lucia LA, Hubbe MA, Pal L (2019) Nanocellulose-based multilayer barrier coatings for gas, oil, and grease resistance. Carbohydr Polym 206:281–288
Zakaria S, Chia CH, Ahmad WA, Kaco H, Chook SW, Chan CH (2015) Mechanical and antibacterial properties of paper coated with chitosan. Sains Malaysiana 44:905–911